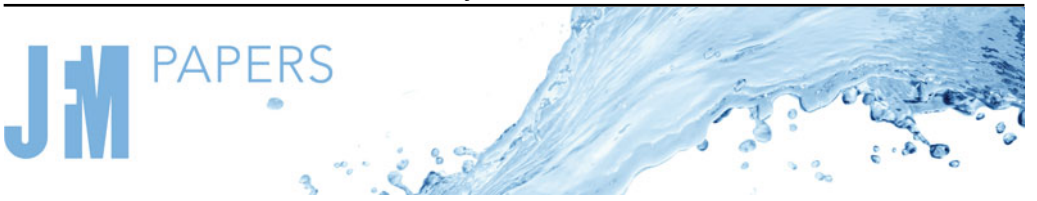
J. Fluid Mech. (2026), *vol.* 1031, A53, doi:10.1017/jfm.2026.11343



Eddy thermal diffusivity model and mean temperature profiles in turbulent vertical convection

Ho Yin Ng[1] **and Emily S.C. Ching**[1]

[1]Department of Physics, The Chinese University of Hong Kong, Shatin, Hong Kong

Corresponding author: Emily S.C. Ching, ching@phy.cuhk.edu.hk

(Received 20 October 2025; revised 13 February 2026; accepted 15 February 2026)

In this paper, we propose a space-dependent eddy thermal diffusivity model for turbulent vertical natural convection in a fluid between two infinite vertical walls at different temperatures. Using this model, we derive analytical results for the mean temperature profile. Our results reveal that mean temperature profiles for different Rayleigh and Prandtl numbers are described by two universal scaling functions in the inner region next to the walls and the outer region near the centreline between the two walls, and the characteristic temperature scales in the inner and outer regions are expressed in terms of the two parameters of the model which determine the characteristic velocities for heat transfer in the two regions. We show that these results are in good agreement with direct numerical simulation data.

Key words: convection in cavities, turbulent convection

1. Introduction

Natural convective flows driven by temperature differences are ubiquitous in nature and engineering applications. To understand buoyancy-driven wall-bounded flows, it is common to study natural convection in a fluid confined between two vertical walls at different temperatures (Batchelor 1954; MacGregor & Emery 1969; Versteegh & Nieuwstadt 1999; Betts & Bokhari 2000; Balaji, Hölling & Herwig 2007; Trias *et al.* 2007; Kiš & Herwig 2012; Ng, Chung & Ooi 2013; Shishkina 2016; Howland *et al.* 2022) or adjacent to a single heated vertical plate (Ostrach 1953; Cheesewright 1968; Kuiken 1968; George & Capp 1979; Ruckenstein & Felske 1980; Tsuji & Nagano 1988; Ke *et al.* 2021). The state of these convective flows is determined by two control parameters, the Rayleigh number (Ra) and Prandtl number (Pr). Laminar vertical convection has

© The Author(s), 2026. Published by Cambridge University Press. This is an Open Access article, distributed under the terms of the Creative Commons Attribution licence (https://creativecommons.org/licenses/by/4.0/), which permits unrestricted re-use, distribution and reproduction, provided the original article is properly cited.

https://doi.org/10.1017/jfm.2026.11343 Published online by Cambridge University Press

been understood by analysis of steady-state boundary-layer equations (Ostrach 1953; Kuiken 1968; Shishkina 2016) but a full understanding of turbulent vertical convection is still lacking. Knowledge of turbulent vertical convection is important for engineering applications such as ventilation in buildings and can shed light on ice–ocean interaction at near-vertical ice surfaces in a polar ocean (Wells & Worster 2008; Howland, Verzicco & Lohse 2023). Physical quantities of interest include heat flux, wall shear stress, maximum mean vertical velocity and mean temperature and velocity profiles.

A recent theoretical analysis by one of us (Ching 2023) showed that, for fluid confined between two infinite vertical walls at different temperatures, the Nusselt number (Nu) and shear Reynolds number (Re_τ), which describe heat flux and wall shear stress, scale as $Ra^{1/3}$ in the high-Ra limit. These theoretical results can well describe direct numerical simulation (DNS) data (Howland *et al.* 2022). The scaling $Nu \sim Ra^{1/3}$ is also consistent with experimental results for fluids with different Pr (Jakob 1949; MacGregor & Emery 1969; Tsuji & Nagano 1988) and the asymptotic law of heat transfer derived by George & Capp (1979) for turbulent natural convection next to a semi-infinite heated vertical plate. The analysis by George & Capp (1979) also yields the mean temperature and velocity profiles. By proposing scaling functions of temperature and velocity of certain characteristic scales of length, velocity and temperature in an inner layer next to the heated plate and a turbulent outer layer far away from the plate and matching them in an overlap layer, which is assumed to exist in the high-Ra limit, they obtained an inverse cubic-root dependence on distance for the mean temperature and a cubic-root dependence for the mean velocity in the overlap layer. The result for the mean velocity deviates from both experimental and DNS data (Versteegh & Nieuwstadt 1999; Hölling & Herwig 2005; Shiri & George 2008). Using a different temperature scale in the inner layer, a logarithmic mean temperature profile was obtained by Hölling & Herwig (2005). The inverse cubic-root and the logarithmic mean temperature profiles have been shown to fit experimental (Cheesewright 1968; Tsuji & Nagano 1988) and DNS data (Versteegh & Nieuwstadt 1999; Ng *et al.* 2013) for air ($Pr = 0.709$) over different spatial regions but their validity for general values of Pr has not been tested. Li *et al.* (2023) studied the mean velocity and temperature profiles using models for turbulent heat flux and Reynolds stress but their models violate required boundary conditions at the vertical walls.

In this paper, we propose a space-dependent eddy thermal diffusivity model for turbulent vertical convection in a fluid between two infinite vertical walls at different temperatures and use it to derive analytical results for the mean temperature profile. These analytical results reveal that mean temperature profiles for different Rayleigh and Prandtl numbers are described by two universal scaling functions in the inner region near the walls and the outer region near the centreline between the two walls. We validate our results using DNS data for $1 \leq Pr \leq 100$ and $10^6 \leq Ra \leq 10^9$ (Howland *et al.* 2022) and show that the two scaling functions can better describe the data than results reported in previous studies.

2. The problem

We consider a fluid confined between two infinite vertical walls separated by a distance H. The wall at the wall-normal coordinate $x = 0$ is kept at a temperature T_h and the wall at $x = H$ at a lower temperature $T_c = T_h - \Delta T$. With the Oberbeck–Boussinesq approximation, the equations governing the fluid motion are $\boldsymbol{\nabla} \cdot \boldsymbol{u} = 0$ and

$$\frac{\partial \boldsymbol{u}}{\partial t} + \boldsymbol{u} \cdot \boldsymbol{\nabla} \boldsymbol{u} = -\frac{1}{\rho} \boldsymbol{\nabla} p + \nu \nabla^2 \boldsymbol{u} + \alpha g (T - T_m) \hat{z}, \tag{2.1}$$

$$\frac{\partial T}{\partial t} + \boldsymbol{u} \cdot \boldsymbol{\nabla} T = \kappa \nabla^2 T, \tag{2.2}$$

https://doi.org/10.1017/jfm.2026.11343 Published online by Cambridge University Press

where $\boldsymbol{u}(x, y, z, t) = (u, v, w)$ is the velocity, $p(x, y, z, t)$ is the pressure, $T(x, y, z, t)$ is the temperature, ρ is the density of the fluid at the temperature at the centreline between the walls, $T_m = (T_h + T_c)/2$, α, ν and κ are the volume expansion coefficient, kinematic viscosity and thermal diffusivity of the fluid, respectively, g is the acceleration due to gravity and $\hat{z}$ is a unit vector along the vertical direction. The velocity field satisfies the no-slip boundary condition at the two walls. The Rayleigh number and the Prandtl number are defined by

$$Ra \equiv \frac{\alpha g \Delta T H^3}{\nu \kappa}, \qquad Pr \equiv \frac{\nu}{\kappa}. \tag{2.3}$$

The flow quantities are Reynolds decomposed into sums of time averages and fluctuations such as $T(x, y, z, t) = \overline{T}(x, y, z) + T'(x, y, z, t)$, where an overbar denotes an average over time and primed symbols denote fluctuating quantities. As the vertical walls are infinite, all the mean flow quantities depend on x only. This is also valid when periodic boundary conditions are imposed on the velocity and temperature in the spanwise (y) and streamwise (z) directions as in DNS (Versteegh & Nieuwstadt 1999; Ng *et al.* 2013; Howland *et al.* 2022). Taking the time average of (2.1) and (2.2) leads to the mean flow equations (Versteegh & Nieuwstadt 1999)

$$\frac{d}{\mathrm{d}x}\overline{u'w'} = \nu \frac{d^2}{\mathrm{d}x^2}\overline{w} + \alpha g(\overline{T} - T_m), \tag{2.4}$$

$$\frac{d}{\mathrm{d}x}\overline{u'T'} = \kappa \frac{d^2}{\mathrm{d}x^2}\overline{T}. \tag{2.5}$$

The boundary conditions are

$$\overline{w}(0) = 0, \qquad \overline{w}(H/2) = 0, \tag{2.6}$$

$$\overline{T}(0) = T_h, \qquad \overline{T}(H/2) = T_m, \tag{2.7}$$

and by symmetry, the mean profiles $\overline{w}(x)$ and $\overline{T}(x)$ are antisymmetric about $x = H/2$. A well-known challenge for solving $\overline{w}(x)$ and $\overline{T}(x)$ is that (2.4) and (2.5) are not closed. In this paper, we focus on finding $\overline{T}$ by solving (2.5) with (2.7) using a closure model for the eddy thermal diffusivity.

3. Eddy thermal diffusivity and mean temperature profiles

3.1. *Eddy thermal diffusivity model*

Integrating (2.5) with respect to x, one obtains

$$\overline{u'T'} - \kappa \frac{\mathrm{d}\overline{T}}{\mathrm{d}x} = -\kappa \frac{\mathrm{d}\overline{T}}{\mathrm{d}x}\bigg|_{x=0} = \kappa Nu \frac{\Delta T}{H}, \tag{3.1}$$

where Nu, being the ratio of the actual heat flux normal to the walls to the heat flux when there is only thermal conduction, is defined by

$$Nu \equiv \frac{\overline{u'T'} - \kappa \mathrm{d}\overline{T}/\mathrm{d}x}{\kappa \Delta T/H} \equiv \frac{q}{\kappa \Delta T/H}. \tag{3.2}$$

The heat flux is given by the product of q and ρc, where c is the specific heat capacity of the fluid. We introduce a space-dependent function $K(x)$ for the eddy thermal diffusivity

$$\overline{u'T'} \equiv -K(x)\frac{\mathrm{d}\overline{T}}{\mathrm{d}x}. \tag{3.3}$$

https://doi.org/10.1017/jfm.2026.11343 Published online by Cambridge University Press

Then (3.1) with (3.3) can be integrated to give (Ruckenstein & Felske 1980)

$$\frac{1}{\Delta T}[\overline{T}(x) - T_m] = \frac{1}{2} - Nu \int_0^{x/H} \frac{\mathrm{d}y}{1 + K(yH)/\kappa}, \tag{3.4}$$

and Nu is obtained by using the boundary condition at $x = H/2$ in (2.7)

$$Nu = \frac{1}{2}\left[\int_0^{1/2} \frac{\mathrm{d}y}{1 + K(yH)/\kappa}\right]^{-1}. \tag{3.5}$$

Thus, both $\overline{T}$ and Nu can be determined if $K(x)$ is known.

The characteristic temperature scales in the inner region near the wall and the outer region near the centreline between the two walls should have different dependencies on ν and κ as molecular diffusivities are expected to play a significant role in the inner region but not the outer region. As seen from (3.4), this suggests that the eddy diffusivity $K(x)$ is governed by two independent parameters in the inner and outer regions. Thus, we model $K(x)$ separately in the inner and outer regions and in the intermediate region between them. Due to the no-slip and isothermal boundary conditions at the two vertical sidewalls, u', T' and $\partial u'/\partial x = -(\partial v'/\partial y + \partial w'/\partial z)$ vanish at $x = 0$, and this leads to the vanishing of $\overline{u'T'}$ and its first- and second-order derivatives with respect to x at $x = 0$ (Ruckenstein & Felske 1980; Ching 2023). Since the temperature gradient at $x = 0$, being proportional to Nu, is non-zero, $K(x)$ and its first- and second-order derivatives should also vanish at $x = 0$. Thus, we model $K(x)/\nu$ by a cubic function in the inner region. In the outer region, we make use of the symmetry of the problem. Since $\overline{u'T'}$ is symmetric and $\overline{T}$ is antisymmetric about the centreline $x = H/2$, $K(x)$ is symmetric about $x = H/2$ and attains a maximum value at $x = H/2$. This motivates us to model $K(x)/\nu$ by the simplest symmetric quadratic function with a peak at $x = H/2$ in the outer region. For the intermediate region, we choose a linear function that connects continuously to the other two regions as it is simple and the resulting $K(x)$ gives rise to a Nu that scales as $Ra^{1/3}$ in the high-Ra limit in accord with the theoretical result (Ching 2023) (cf. § 4). Putting all these results together, we propose a three-layer model for $K(x)/\nu$

$$\frac{K(x)}{\nu} = \begin{cases} Ay^3, & 0 \le y \le y_1, \\ c_1 + c_2 y, & y_1 < y < y_2, \\ C_m[1 - b(1/2 - y)^2], & y_2 \le y \le 1/2, \end{cases} \tag{3.6}$$

where $y = x/H$. Near the walls, the turbulent heat flux is expected to be small compared with the conductive heat flux, or equivalently, $K(x)$ is expected to be small compared with κ. Thus, a natural characteristic length scale for the inner region is given by

$$l_i = \frac{H}{(PrA)^{1/3}}, \tag{3.7}$$

which is the position at which our proposed model of eddy thermal diffusivity is equal to κ, and we set the width of the inner region to be $2l_i$, i.e. $y_1 H = 2l_i$. We note that the equality of the eddy and molecular thermal diffusivities was used to define the thickness of the thermal boundary layer in vertical convection by Howland *et al.* (2022). We fix the width of the outer region to be $0.2H$ with $y_2 = 0.3$ and take $b = 4$. These values are guided by the DNS data (Howland *et al.* 2022). The constants c_1 and c_2 are fixed by the continuity of $K(x)/\nu$ at $x = y_1 H$ and $x = y_2 H$

$$c_1 = \frac{Ay_1^3 y_2 - C_m\left[1 - b(1/2 - y_2)^2\right] y_1}{y_2 - y_1}, \quad c_2 = \frac{C_m\left[1 - b(1/2 - y_2)^2\right] - Ay_1^3}{y_2 - y_1}. \tag{3.8}$$

https://doi.org/10.1017/jfm.2026.11343 Published online by Cambridge University Press

Hence, the model has two independent parameters: A and C_m. We will show below that they determine the characteristic velocities for heat transfer in the inner and outer regions, respectively.

3.2. *Mean temperature profiles*

Substituting (3.6) into (3.4) and evaluating the integral, we obtain $\overline{T}(x)$

$$\frac{1}{\Delta T}[T_h - \overline{T}(yH)] = \begin{cases} Nu\, I_1(y), & 0 \le y \le y_1, \\ Nu\,[I_1(y_1) + I_2(y)], & y_1 < y < y_2, \end{cases} \tag{3.9}$$

$$\frac{1}{\Delta T}[\overline{T}(yH) - T_m] = Nu\, I_3(y), \qquad y_2 \le y \le 1/2, \tag{3.10}$$

where

$$Nu = \frac{1}{2[I_1(y_1) + I_2(y_2) + I_3(y_2)]}, \tag{3.11}$$

and

$$I_1(y) \equiv \frac{1}{Pr^{\frac{1}{3}} A^{\frac{1}{3}}} \int_0^{Pr^{1/3}A^{1/3}y} \frac{\mathrm{d}y'}{1+y'^3} = \frac{1}{3Pr^{\frac{1}{3}} A^{\frac{1}{3}}} \left\{ \frac{1}{2} \log \left[\frac{\left(1 + Pr^{\frac{1}{3}} A^{\frac{1}{3}} y\right)^3}{1 + PrAy^3} \right] + \sqrt{3} \arctan\left(\frac{2Pr^{\frac{1}{3}} A^{\frac{1}{3}} y - 1}{\sqrt{3}} \right) + \frac{\sqrt{3}\pi}{6} \right\}, \tag{3.12}$$

$$I_2(y) \equiv \int_{y_1}^{y} \frac{\mathrm{d}y'}{1 + Pr(c_1 + c_2 y')} = \frac{1}{Prc_2} \log \left[\frac{1 + Pr(c_1 + c_2 y)}{1 + Pr(c_1 + c_2 y_1)} \right], \tag{3.13}$$

$$I_3(y) \equiv \int_y^{1/2} \frac{\mathrm{d}y'}{1 + PrC_m[1 - b(1/2 - y')^2]} = \frac{1}{2B(1 + C_m Pr)} \log \left| \frac{1 + B(1/2 - y)}{1 - B(1/2 - y)} \right|, \quad B = \sqrt{bC_m Pr/(1 + C_m Pr)}. \tag{3.14}$$

We focus on the mean temperature profile in the inner and outer regions. The analytical results (3.9) and (3.10) reveal that $\overline{T}(x)$ is given by two universal scaling functions of their respective characteristic temperature and length scales in these two regions, namely

$$T_h - \overline{T}(x) = T_i F_i(x/l_i) \qquad \text{inner wall region}, \tag{3.15}$$

$$\overline{T}(x) - T_m = T_o F_o(x/H) \qquad \text{outer centreline region}, \tag{3.16}$$

where the inner and outer scaling functions are

$$F_i(z) = \frac{1}{6} \log \left[\frac{(1+z)^3}{1+z^3} \right] + \frac{\sqrt{3}}{3} \arctan\left(\frac{2z-1}{\sqrt{3}} \right) + \frac{\sqrt{3}\pi}{18}, \tag{3.17}$$

$$F_o(z) = \frac{1}{2\sqrt{b}} \log \left| \frac{1 + \sqrt{b}(1/2 - z)}{1 - \sqrt{b}(1/2 - z)} \right| = \frac{1}{4} \log \left(\frac{1-z}{z} \right), \tag{3.18}$$

the inner and outer temperature scales are

$$T_i = \frac{\Delta T Nu}{(PrA)^{1/3}}, \tag{3.19}$$

$$T_o = \frac{\Delta T Nu}{PrC_m}, \tag{3.20}$$

https://doi.org/10.1017/jfm.2026.11343 Published online by Cambridge University Press

and the characteristic length scales in the inner and outer regions are l_i and H, respectively. To obtain (3.16) with (3.18), we have used the approximation $PrC_m \gg 1$, which follows from the dominance of the turbulent heat flux over the conductive heat flux, $|\overline{u'T'}| \gg \kappa|\mathrm{d}\overline{T}/\mathrm{d}x|$, at $x = H/2$ in the outer region for turbulent convective flows. Using (3.2) and (3.7), we can rewrite (3.19) and (3.20) as

$$V_i T_i = V_o T_o = q, \tag{3.21}$$

where

$$V_i \equiv \frac{\kappa}{l_i} = \frac{\kappa}{H}(PrA)^{1/3}, \tag{3.22}$$

$$V_o \equiv \frac{K(H/2)}{H} = \frac{\nu C_m}{H}. \tag{3.23}$$

Thus, the two parameters A and C_m determine V_i and V_o, the characteristic velocities for heat transfer in the inner and outer regions, respectively.

4. Validation and discussions

4.1. *Validation*

Using DNS data for $Pr = 1$, 2, 5, 10 and 100 and Ra ranging from 10^6 to 10^9 (Howland *et al.* 2022), we evaluate $K(x)/\nu$, we fit it by $A(x/H)^3$ in the region $0 \le x/H \le 2l_i/H = 2/(PrA)^{1/3}$ using the least-square method to obtain A and extract C_m directly as $C_m = K(H/2)/\nu$. The values of A and C_m are shown in table 1. In determining $\overline{T}(x)$ and Nu, the relevant quantity is $F(x) = 1/[1 + PrK(x)/\nu]$ (see (3.4) and (3.5)). We compare $F(x)$ evaluated using the eddy diffusivity model (3.6) and the DNS data in figure 1. Good agreement can be seen, which is further supported by the relatively small errors of the values of Nu estimated using the model with respect to the DNS data (see table 1). Good agreement between the analytical result for $\overline{T}$ and the DNS data is also shown in figure 1. If $K(x)/\nu$ is modelled by $A(x/H)^3$ throughout the whole region (Ruckenstein & Felske 1980), the estimated Nu would be given by $1/[2I_1(1/2)]$. As shown in table 1, the relative errors of these estimates of Nu are substantially larger for $Pr \le 5$.

In figure 2, we plot $(T_h - \overline{T})/T_i$ as a function of x/l_i. The DNS data for different Pr and Ra collapse onto a single curve that is well described by the theoretical inner scaling function F_i in (3.17) for $0 \le x/l_i < 2$, validating (3.15). In this region, F_i clearly deviates from a linear function, showing that the turbulent heat flux $\overline{u'T'}$ cannot be neglected even within the inner region. Following George & Capp (1979), we express the temperature and length scales in the inner region in terms of heat flux, or equivalently, q, the buoyancy parameter αg and the molecular diffusivities ν and κ. Dimensional analysis then yields

$$T_i = \left(\frac{q^3}{\alpha g \kappa}\right)^{\frac{1}{4}} g_i(Pr) = T_{i,GC} g_i(Pr) = \Delta T Nu^{3/4} (RaPr)^{-\frac{1}{4}} g_i(Pr), \tag{4.1}$$

up to some Pr-dependent function $g_i(Pr)$. Using (3.21) and (3.22), we have

$$l_i = \left(\frac{\kappa^3}{\alpha g q}\right)^{\frac{1}{4}} g_i(Pr) = l_{i,GC} g_i(Pr). \tag{4.2}$$

Our inner temperature and length scales T_i and l_i thus differ from the scales $T_{i,GC} = (q^3/\alpha g \kappa)^{1/4}$ and $l_{i,GC} = (\kappa^3/\alpha g q)^{1/4}$ adopted by George & Capp (1979). The inclusion of ν in our analysis leads to an additional function $g_i(Pr)$, and this enables us to obtain a

https://doi.org/10.1017/jfm.2026.11343 Published online by Cambridge University Press

Pr	Ra	A	C_m	Nu (DNS)	Nu (model)	$1/[2I_1(1/2)]$
1	1×10^6	10478.14	30.77	6.59	7.22 (9.51 %)	9.08 (37.70 %)
1	2×10^6	22731.58	41.78	8.30	9.06 (9.12 %)	11.74 (41.36 %)
1	5×10^6	56711.28	60.42	11.31	11.92 (5.38 %)	15.90 (40.66 %)
1	1×10^7	109126.23	80.68	13.81	14.63 (5.91 %)	19.77 (43.18 %)
1	2×10^7	225663.87	109.19	17.10	18.34 (7.23 %)	25.19 (47.28 %)
1	5×10^7	521909.56	168.07	22.93	24.40 (6.39 %)	33.30 (45.21 %)
1	1×10^8	972659.79	221.83	28.19	29.91 (6.10 %)	40.98 (45.34 %)
2	1×10^6	3971.13	18.90	6.50	7.05 (8.38 %)	8.28 (27.40 %)
2	2×10^6	8504.98	26.17	8.28	8.88 (7.30 %)	10.66 (28.79 %)
2	5×10^6	23296.22	40.00	11.25	12.12 (7.67 %)	14.90 (32.39 %)
2	1×10^7	43690.91	54.01	14.11	14.85 (5.27 %)	18.36 (30.14 %)
2	2×10^7	87605.10	72.54	17.57	18.52 (5.39 %)	23.15 (31.73 %)
2	5×10^7	204899.56	107.28	23.41	24.49 (4.62 %)	30.72 (31.25 %)
2	1×10^8	419021.34	141.89	29.07	30.72 (5.68 %)	38.99 (34.13 %)
5	1×10^6	1215.97	8.56	6.10	6.74 (10.55 %)	7.58 (24.38 %)
5	2×10^6	2424.42	12.39	7.82	8.42 (7.65 %)	9.53 (21.84 %)
5	5×10^6	5834.48	21.25	10.76	11.35 (5.52 %)	12.75 (18.54 %)
5	1×10^7	11543.18	28.71	13.61	14.12 (3.78 %)	16.00 (17.58 %)
5	2×10^7	22446.05	39.75	17.08	17.59 (3.00 %)	19.96 (16.84 %)
5	5×10^7	55357.57	60.42	23.01	23.71 (3.06 %)	26.96 (17.17 %)
5	1×10^8	107172.05	79.49	28.64	29.40 (2.64 %)	33.59 (17.29 %)
10	1×10^6	372.05	3.50	5.36	5.82 (8.45 %)	6.45 (20.28 %)
10	2×10^6	835.21	6.08	7.22	7.65 (5.97 %)	8.42 (16.67 %)
10	5×10^6	2062.50	11.98	10.09	10.54 (4.47 %)	11.36 (12.66 %)
10	1×10^7	3955.05	17.98	12.72	13.18 (3.63 %)	14.11 (10.92 %)
10	2×10^7	7875.63	23.67	16.05	16.43 (2.37 %)	17.74 (10.55 %)
10	5×10^7	19137.64	39.09	21.71	22.29 (2.64 %)	23.84 (9.80 %)
10	1×10^8	37057.30	50.27	27.13	27.59 (1.69 %)	29.71 (9.52 %)
10	2×10^8	72836.27	67.87	33.89	34.54 (1.91 %)	37.21 (9.80 %)
10	5×10^8	167572.38	98.02	45.20	45.61 (0.91 %)	49.12 (8.66 %)
10	1×10^9	333601.74	129.57	55.91	57.27 (2.43 %)	61.79 (10.52 %)
100	1×10^7	51.94	0.88	7.86	7.02 (10.63 %)	7.20 (8.33 %)
100	2×10^7	151.22	2.05	10.81	10.19 (5.73 %)	10.25 (5.18 %)
100	5×10^7	354.76	4.57	15.09	13.88 (8.01 %)	13.61 (9.82 %)
100	1×10^8	784.51	7.00	19.16	18.12 (5.43 %)	17.72 (7.55 %)
100	2×10^8	1550.46	11.36	24.35	22.97 (5.69 %)	22.23 (8.72 %)
100	5×10^8	3338.95	18.75	32.32	29.91 (7.47 %)	28.70 (11.21 %)
100	1×10^9	6491.31	26.64	40.14	37.44 (6.71 %)	35.81 (10.78 %)

Table 1. Values of the parameters A and C_m of the eddy thermal diffusivity model. Here, Nu (model) are the Nu values estimated using the eddy diffusivity model with these values of A and C_m and $1/[I_1(1/2)]$ are the values of Nu obtained when $K(x)/\nu$ is modelled instead by $A(x/H)^3$. The numbers in parentheses are the relative errors of the estimated values of Nu with respect to the DNS data by Howland *et al.* (2022).

universal scaling function F_i in the inner region for all Pr. By comparing (3.19) with (4.1), we obtain

$$(PrA)^{-1/3} = (RaPrNu)^{-1/4} g_i(Pr), \tag{4.3}$$

which is used to evaluate $g_i(Pr)$. We find that $g_i(Pr)$ can be fitted by a power law $k_i Pr^{\beta}$ with $\beta = 0.425 \approx 3/7$ and $k_i = 2.18$. A commonly used velocity scale in the inner region is the friction velocity $u_\tau = \sqrt{\nu \mathrm{d}\overline{w}/\mathrm{d}x|_{x=0}}$. It is interesting to compare the inner velocity

https://doi.org/10.1017/jfm.2026.11343 Published online by Cambridge University Press

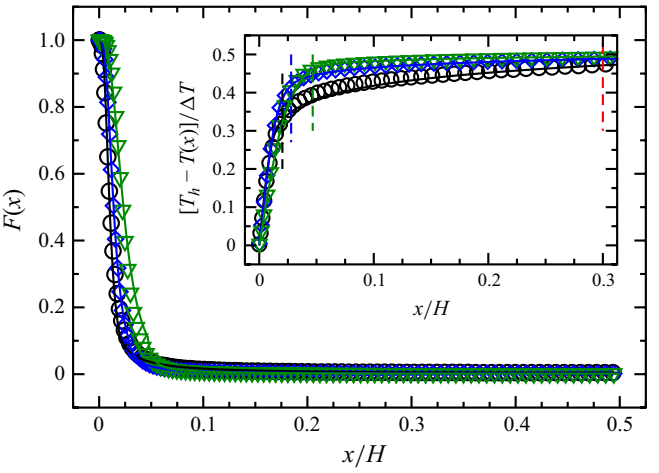


Figure 1. Value of $F(x) = 1/[1 + PrK(x)/\nu]$ vs x at $Ra = 10^8$ for $Pr = 1$ (black), $Pr = 10$ (blue) and $Pr = 100$ (green). The symbols are DNS data (Howland *et al.* 2022) and the solid lines are evaluated using the eddy diffusivity model (3.6) with the values of A and C_m from table 1. In the inset, we compare the analytical result of the mean temperature profiles $\overline{T}(x)$ from the model (solid lines) with the DNS data. The dashed lines denote the positions of y_1 and $y_2 = 0.3$.

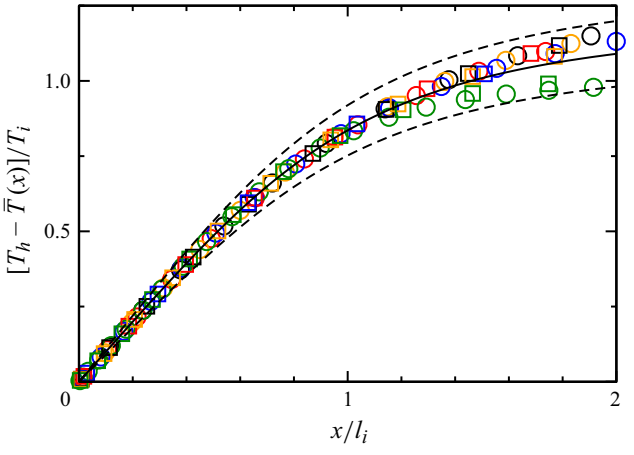


Figure 2. Value of $(T_h - \overline{T})/T_i$ vs x/l_i at Ra_{min} (circles) and Ra_{max} (squares) for $Pr = 1$ (black), $Pr = 2$ (red), $Pr = 5$ (orange), $Pr = 10$ (blue) and $Pr = 100$ (green). Here, Ra_{min} and Ra_{max} are the minimum and maximum values of Ra for the corresponding Pr (see table 1). The solid line is the inner scaling function F_i given by (3.17) and the two dashed lines indicate $0.9F_i$ and $1.1F_i$.

scale V_i and u_τ. Using (3.22) and (4.3), we obtain

$$\frac{V_i}{u_\tau} = \frac{(RaNu)^{1/4}}{g_i(Pr)Pr^{3/4}Re_\tau}, \tag{4.4}$$

where $Re_\tau = u_\tau H/\nu$ is the shear Reynolds number. The theoretical results of Ching (2023) that Nu and Re_τ scale as $Ra^{1/3}$ in the high-Ra limit then imply that V_i is related to u_τ by a Pr-dependent function $h(Pr)$ when Ra is sufficiently large

$$V_i \approx h(Pr)u_\tau. \tag{4.5}$$

https://doi.org/10.1017/jfm.2026.11343 Published online by Cambridge University Press

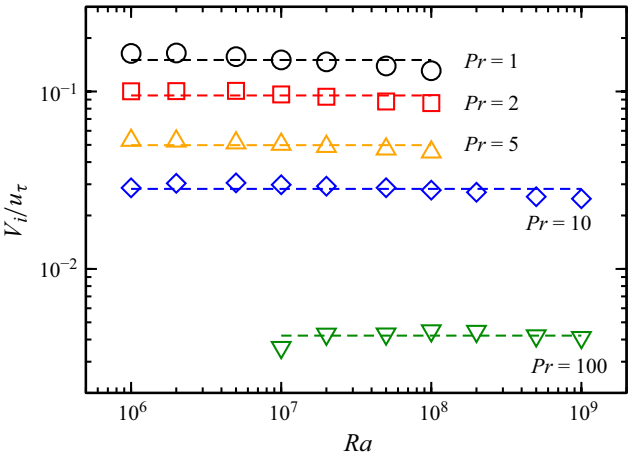


Figure 3. Value of V_i/u_τ as a function of Ra. The dashed lines give the average values of V_i/u_τ over Ra for each Pr.

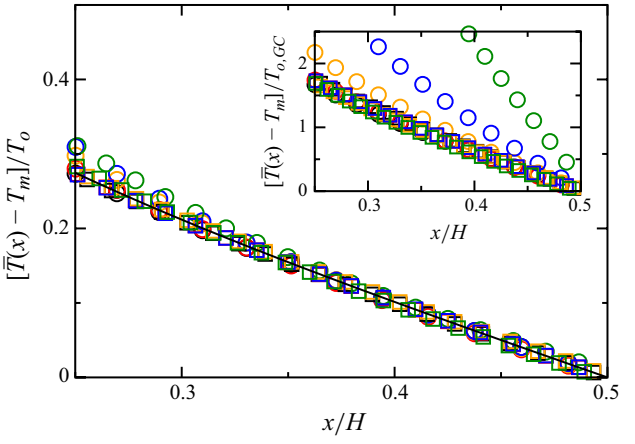


Figure 4. Plot of $(\overline{T} - T_m)/T_o$ vs x/H at Ra_{min} and Ra_{max} for $Pr = 1, 2, 5, 10, 100$. Same symbols as in figure 2. The solid line is the function F_o given by (3.18). A similar plot is shown in the inset with the temperature rescaled by $T_{o,GC}$ instead of T_o.

It can be seen in figure 3 that (4.5) is confirmed and $h(Pr)$ is a decreasing function of Pr. As a result, if the mean temperature profiles are rescaled by $l_\tau \equiv \kappa/u_\tau$ and $T_\tau \equiv q/u_\tau$ instead of l_i and T_i, the profiles for different Pr do not collapse beyond the linear region near the wall (as shown in figure 5*b* of Howland *et al.* 2022).

Next we check (3.16). As shown in figure 4, the rescaling of $\overline{T} - T_m$ by T_o results in an approximate collapse of the data in the region $0.3 \leq x/H \leq 0.5$. The collapsed data are consistent with the outer scaling function F_o with $b = 4$ in (3.18). These observations support our choice of $y_2 = 0.3$ and $b = 4$ and validate our proposed functional form of $K(x)$ in the outer region. If the outer temperature scale $T_{o,GC}$ proposed by George & Capp (1979) is used instead of T_o, the data collapse is worse (see the inset of figure 4). The scale $T_{o,GC}$, given by

$$T_{o,GC} = \left(\frac{q^2}{\alpha g H}\right)^{1/3}, \tag{4.6}$$

https://doi.org/10.1017/jfm.2026.11343 Published online by Cambridge University Press

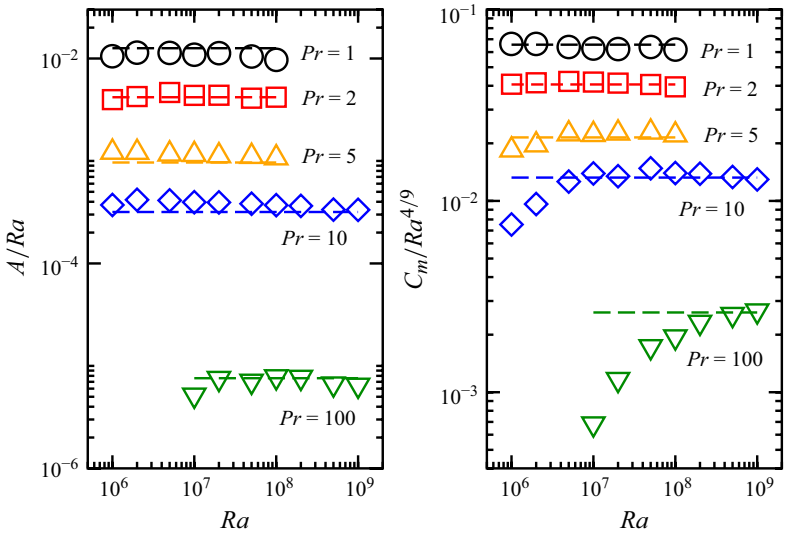


Figure 5. Plot of A/Ra and $C_m/Ra^{4/9}$ vs Ra.The dashed lines for different Pr are the values of $C_1(Pr)$ and $C_2(Pr)$ obtained by using $C = 0.043$, $f(Pr) \approx 0.19$ (Ching 2023) and the fitted values of k_i, β and k_o (see (4.9) and (4.10)).

was obtained by assuming that the temperature scale in the outer region depends on q, αg and H only and not on the molecular diffusivities ν and κ. We find that

$$C_m \to k_o(RaNu)^{1/3}Pr^{-2/3}, \tag{4.7}$$

with $k_o = 0.162$ for sufficiently large Ra. This implies that $T_o \to k_o^{-1}T_{o,GC}$ when Ra is greater than certain threshold value $Ra_c(Pr)$ and $Ra_c(Pr)$ increases with Pr.

Finally, we show that our model gives $Nu \sim Ra^{1/3}$ in the high-Ra limit. Using (4.3) and (4.7), it can be shown that, for sufficiently large Ra, $I_1(y_1) \sim (RaNu)^{-1/4}$, $I_2(y_2) \sim (RaNu)^{-1/3}\ln(RaNu)$ and $I_3(y_2) \sim (RaNu)^{-1/3}$ and hence

$$Nu \approx \frac{1}{2I_1(y_1)} \Rightarrow Nu \sim Ra^{1/3}. \tag{4.8}$$

Substituting the theoretical result of $Nu \approx [C^2 f(Pr)]^{1/3}Pr^{-1/9}Ra^{1/3} = \gamma(Pr)Ra^{1/3}$ for $Pr \geq 1$ in the high-Ra limit (Ching 2023) into (4.3) and (4.7), we obtain

$$A \approx [\gamma(Pr)]^{3/4}[g_i(Pr)]^{-3}Pr^{-1/4}Ra = C_1(Pr)Ra, \tag{4.9}$$

$$C_m \approx k_o[\gamma(Pr)]^{1/3}Pr^{-2/3}Ra^{4/9} = C_2(Pr)Ra^{4/9}, \tag{4.10}$$

when Ra is sufficiently large. Such Ra-dependencies of A and C_m are confirmed in figure 5.

4.2. *Comparison with mean temperature profiles reported in previous studies*

One often-cited result for the mean temperature profile was obtained by George & Capp (1979). They proposed scaling functions in terms of $T_{i,GC}$ and $l_{i,GC}$ in the inner region and $T_{o,GC}$ and H in the outer region. In an overlap layer in which both scaling functions hold, they obtained

$$\frac{T_h - \overline{T}(x)}{T_{i,GC}} = -K_1\left(\frac{x}{l_{i,GC}}\right)^{-1/3} + \phi_1(Pr), \tag{4.11}$$

https://doi.org/10.1017/jfm.2026.11343 Published online by Cambridge University Press

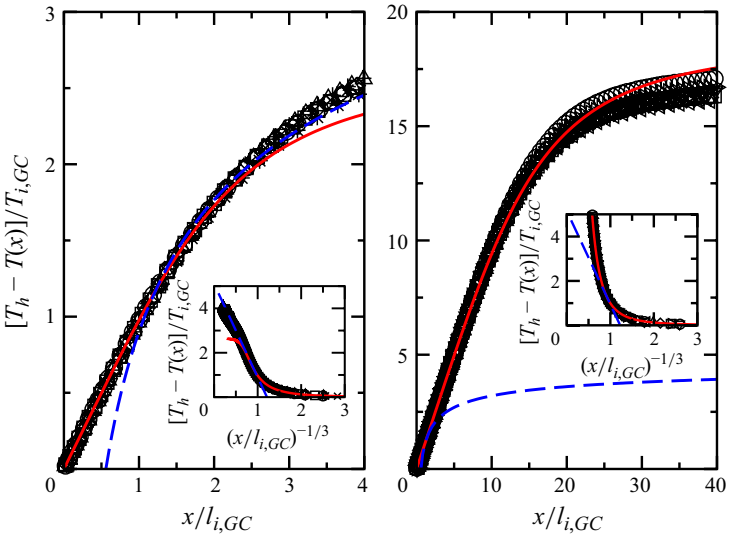


Figure 6. Plots of $[T_h - \overline{T}(x)]/T_{i,GC}$ vs $x/l_{i,GC}$ for $Pr = 1$ (left panel) and $Pr = 100$ (right panel) at $Ra = 10^6$ (plusses), 2×10^6 (crosses), 5×10^6 (stars), 10^7 (circles), 2×10^7 (squares), 5×10^7 (diamonds), 10^8 (triangles), 2×10^8 (left triangles), 5×10^8 (inverted triangles) and 10^9 (right triangles). The red solid lines are (4.13) and the blue dashed lines are (4.11) with $K_1 = 4.2$, $\phi_1(1) = 5.10$ and $\phi_1(100) = 5.15$.

$$\frac{\overline{T}(x) - T_m}{T_{o,GC}} = K_1 \left(\frac{x}{H}\right)^{-1/3} + \theta_1, \tag{4.12}$$

with undetermined constants K_1, $\phi_1(Pr)$ and θ_1; the independence of K_1 and θ_1 from Pr follows from the independence of the outer scaling function from ν or κ. Fitting their DNS data for $Pr = 0.709$ (air), Versteegh & Nieuwstadt (1999) and Ng *et al.* (2013) found $K_1 = 4.2$. Using the DNS data of Howland *et al.* (2022), we find that the region that (4.11) with $K_1 = 4.2$ can fit decreases drastically for larger Pr while our result for the inner region (3.15) with (3.17), rewritten as

$$\frac{T_h - \overline{T}(x)}{T_{i,GC}} = g_i(Pr) F_i \left(\frac{1}{g_i(Pr)} \frac{x}{l_{i,GC}}\right), \tag{4.13}$$

can give good fits for all the 5 values of Pr studied. The comparison for $Pr = 1$ and $Pr = 100$ is shown in figure 6.

Using the same approach but with the temperature scale $T_{i,GC}$ for both the inner and outer regions, Hölling & Herwig (2005) obtained a logarithmic profile in the overlap layer

$$\frac{T_h - \overline{T}(x)}{T_{i,GC}} = K_2 \log\left(\frac{x}{l_{i,GC}}\right) + \phi_2(Pr), \tag{4.14}$$

$$\frac{\overline{T}(x) - T_m}{T_{i,GC}} = -K_2 \log\left(\frac{x}{H}\right) + \theta_2, \tag{4.15}$$

with undetermined constants K_2, $\phi_2(Pr)$ and θ_2. Different values of K_2 and ϕ_2, obtained by fitting DNS data for air, were reported (Versteegh & Nieuwstadt 1999; Hölling & Herwig 2005; Kiš & Herwig 2012; Ng *et al.* 2013). We thus test instead the relation between Nu, Ra and Pr, obtained by adding (4.14) and (4.15) and using (4.1) and (4.2)

$$(Nu^{-3} RaPr)^{1/4} = \frac{K_2}{2} \log(NuRaPr) + 2[\phi_2(Pr) + \theta_2]. \tag{4.16}$$

https://doi.org/10.1017/jfm.2026.11343 Published online by Cambridge University Press

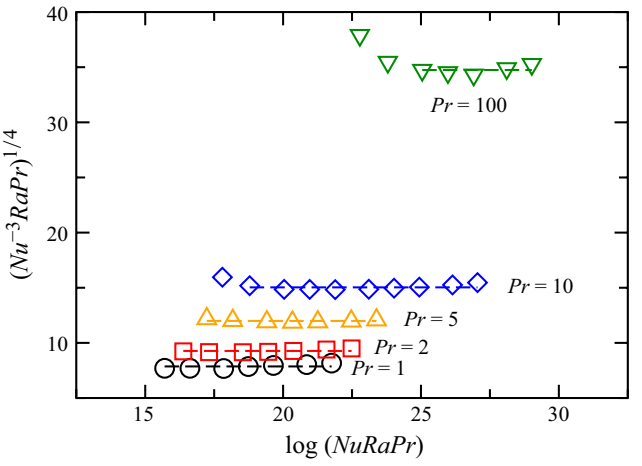


Figure 7. Plot of $(Nu^{-3}RaPr)^{1/4}$ vs $\log(NuRaPr)$ using DNS data of Howland *et al.* (2022). The dashed lines for different Pr are the best fits of (4.16) with $K_2 = 0$.

Balaji, Hölling & Herwig (2007) assumed (4.14) to hold up to $x = H/2$ and obtained a different relation than (4.16). As shown in figure 7, the DNS data (Howland *et al.* 2022) are consistent with (4.16) with $K_2 = 0$, indicating their incompatibility with (4.14) and (4.15). When $K_2 = 0$, (4.16) reduces to $Nu \sim Ra^{1/3}$.

A recent work (Li *et al.* 2023) studied the mean velocity and temperature profiles by modelling the Reynolds stress and turbulent heat flux

$$\overline{u'w'} = -k_1 x^2 \left(\frac{\partial \overline{w}}{\partial x}\right)^2, \tag{4.17}$$

$$\overline{u'T'} = -k_2 x^2 \frac{\partial \overline{w}}{\partial x}\frac{\partial \overline{T}}{\partial x}, \tag{4.18}$$

where k_1 and k_2 are dimensionless coefficients. As discussed in § 3.1, $\overline{u'T'}$ and its first- and second-order derivatives with respect to x vanish at $x = 0$ due to the boundary conditions. Similar arguments require $\overline{u'w'}$ and its first- and second-order derivatives with respect to x to vanish at $x = 0$. These properties should be satisfied by any closure model but they are violated by (4.17) and (4.18). Since both the mean velocity and temperature gradients, $\partial\overline{w}/\partial x$ and $\partial\overline{T}/\partial x$, are non-zero at $x = 0$, the model expressions on the right-hand side of (4.17) and (4.18) have non-vanishing second-order derivatives at $x = 0$. Applying (4.17) and (4.18) to the near-centreline outer region, Li *et al.*, obtained an inverse cubic-root dependence for the mean temperature profile ((2.14*b*) of Li *et al.* 2023), which we rewrite as

$$\frac{\overline{T}(x) - T_m}{T_\tau} = cK\left[\left(\frac{x}{H}\right)^{-1/3} - 2^{1/3}\right] = cKx^*, \tag{4.19}$$

where $K = (\alpha g H T_\tau/u_\tau^2)^{1/3}$, $c \approx 3.8$ and

$$x^* \equiv \left(\frac{x}{H}\right)^{-1/3} - 2^{1/3}. \tag{4.20}$$

We note that (4.19) implies that the mean temperature profiles in the outer region would collapse onto a straight line in x^* when temperature is rescaled by $T_\tau/K = T_{o,GC}$.

https://doi.org/10.1017/jfm.2026.11343 Published online by Cambridge University Press

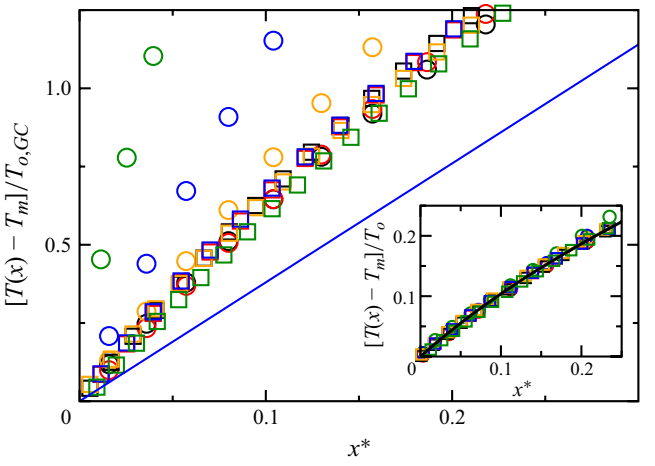


Figure 8. Plot of $(\overline{T} - T_m)/(T_{o,GC})$ vs x^* at Ra_{min} and Ra_{max} for $Pr = 1, 2, 5, 10, 100$. Same symbols as in figure 2 and the solid straight line is cx^*. In the inset, a similar plot is shown with the temperature rescaled by T_o instead of $T_{o,GC}$ and the solid line is (4.21).

Using (4.20), we rewrite our result for the outer region, (3.16) with (3.18), in terms of x^*

$$\frac{\overline{T}(x) - T_m}{T_o} = \frac{1}{4} \log \left[\left(x^* + 2^{1/3} \right)^3 - 1 \right]. \tag{4.21}$$

In figure 8, it can be clearly seen that the mean temperature profiles in the outer region do not collapse onto the straight line cx^* when rescaled by $T_{o,GC}$, contrary to the prediction by (4.19), but they are well represented by (4.21).

5. Conclusions

In this study, we focus on determining the mean temperature profiles in turbulent natural convection between two infinite vertical walls at different temperatures. A three-layer model for the eddy thermal diffusivity with two parameters has been proposed. Using this model, we have derived analytical results for the mean temperature profiles in terms of the two parameters of the model. These analytical results reveal that the mean temperature profiles for different Ra and Pr are described by two universal scaling functions in the inner region next to the walls and the outer region near the centreline between the walls. The characteristic temperature scales in these two regions are expressed in terms of the two parameters, which determine the characteristic velocities for heat transfer in the two regions. The dependencies of the two parameters on Ra and Pr are obtained. Analytical expressions of the two scaling functions are fully determined and there is no overlap region in which both functions hold. Our theoretical results for the mean temperature profiles in the inner and outer regions are in good agreement with DNS data for $1 \leq Pr \leq 100$ and $10^6 \leq Ra \leq 10^9$ (Howland *et al.* 2022) and can give a better description of the data than results reported in the literature (George & Capp 1979; Hölling & Herwig 2005; Li *et al.* 2023).

Funding. This work was funded by the Hong Kong Research Grants Council (Grant No. CUHK 14303623).

Declaration of interests. The authors report no conflicts of interest.

https://doi.org/10.1017/jfm.2026.11343 Published online by Cambridge University Press

References

Balaji, C., Hölling, M. & Herwig, H. 2007 Nusselt number correlations for turbulent natural convection flows using asymptotic analysis of the near-wall region. *ASME J. Heat Transfer* **129**, 1100–1105.

Batchelor, G.K. 1954 Heat transfer by free convection across a closed cavity between vertical boundaries at different temperatures. *Q. Appl. Maths* **12**, 209–233.

Betts, P. & Bokhari, I. 2000 Experiments on turbulent natural convection in an enclosed tall cavity. *Intl J. Heat Fluid Flow* **21**, 675–683.

Cheesewright, R. 1968 Turbulent natural convection from a vertical plane surface. *J. Heat Transfer* **90**, 1–8.

Ching, E.S.C. 2023 Heat flux and wall shear stress in large-aspect-ratio turbulent vertical convection. *Phys. Rev. Fluids* **8**, L022601.

George, W.K.J. & Capp, S.P. 1979 A theory for natural convection turbulent boundary layers next to heated vertical surfaces. *Intl J. Heat Mass Transfer* **22**, 813–826.

Hölling, M. & Herwig, H. 2005 Asymptotic analysis of the near-wall region of turbulent natural convection flows. *J. Fluid Mech.* **541**, 383–397.

Howland, C.J., Ng, C.S., Verzicco, R. & Lohse, D. 2022 Boundary layers in turbulent vertical convection at high Prandtl number. *J. Fluid Mech.* **930**, A32.

Howland, C.J., Verzicco, R. & Lohse, D. 2023 Double-diffusive transport in multicomponent vertical convection. *Phys. Rev. Fluids* **8**, 013501.

Jakob, M. 1949 *Heat Transfer*. Wiley & Sons.

Ke, J., Williamson, N., Armfield, S.W., Komiya, A. & Norris, S.E. 2021 High Grashof number turbulent natural convection on an infinite vertical wall. *J. Fluid Mech.* **929**, A15.

Kiš, P. & Herwig, H. 2012 The near wall physics and wall functions for turbulent natural convection. *Intl J. Heat Mass Transfer* **55**, 2625–2635.

Kuiken, H.K. 1968 An asymptotic solution for large Prandtl number free convection. *J. Engng Maths* **2**, 355–371.

Li, M., Jia, P., Liu, H., Jiao, Z. & Zhang, Y. 2023 Mean velocity and temperature profiles in turbulent vertical convection. *J. Fluid Mech.* **977**, A51.

MacGregor, R.K. & Emery, A.F. 1969 Free convection through vertical plane layers — moderate and high Prandtl number fluids. *Trans. ASME J. Heat Transfer* **93**, 253.

Ng, C.S., Chung, D. & Ooi, A. 2013 Turbulent natural convection scaling in a vertical channel. *Intl J. Heat Fluid Flow* **44**, 554–562.

Ostrach, S. 1953 An analysis of laminar free-convection flow and heat transfer about a flat plate parallel to the direction of the generating body force. *NACA Rep.* 1111, p. 63.

Ruckenstein, E. & Felske, J.D. 1980 Turbulent natural convection at high Prandtl numbers. *ASME J. Heat Transfer* **102**, 773–775.

Shiri, A. & George, W.K. 2008 Turbulent natural convection in a differentially heated vertical channel. In *Proceedings of 2008 ASME Summer Heat Transfer Conference*, pp. 285–291. ASME.

Shishkina, O. 2016 Momentum and heat transport scalings in laminar vertical convection. *Phys. Rev. E* **93**, 051102(R).

Trias, F.X., Soria, M., Oliva, A. & P'erez-Segarra, C.D. 2007 Direct numerical simulations of two- and three-dimensional turbulent natural convection flows in a differentially heated cavity of aspect ratio 4. *J. Fluid Mech.* **586**, 259–293.

Tsuji, T. & Nagano, Y. 1988 Characteristics of a turbulent natural convection boundary layer along a vertical flat plate. *Intl J. Heat Mass Transfer* **31**, 1723–1734.

Versteegh, T.A.M. & Nieuwstadt, F.T.M. 1999 A direct numerical simulation of natural convection between two infinite vertical differentially heated walls scaling laws and wall functions. *Intl J. Heat Mass Transfer* **42**, 3673–3693.

Wells, A.J. & Worster, M.G. 2008 A geophysical-scale model of vertical natural convection boundary layers. *J. Fluid Mech.* **609**, 111–137.

https://doi.org/10.1017/jfm.2026.11343 Published online by Cambridge University Press